2022

Smart Low-cost Thermal Imaging Acquisition Towards Personal Comfort Prediction

Ati Soleimanijavid

Iason Konstantzos

Smart Low-cost Thermal Imaging Acquisition Towards Personal Comfort Prediction

Ati Soleimanijavid[1]*, Iason Konstantzos[1]

[1]Durham School of Architectural Engineering and Construction, University of Nebraska - Lincoln, Omaha, NE, USA
asoleimanijavid2@huskers.unl.edu – iason.konstantzos@unl.edu

* Corresponding Author

ABSTRACT

Ensuring occupants' thermal comfort is rapidly becoming an essential objective in building design and operation, as it plays a crucial role in well-being and productivity. Conventional HVAC system controllers operate based on predefined setpoints and schedules, or individuals' selections. However, as thermal sensation may vary, not only from person to person but also differ over time, the automated operation needs to be informed by real-time sensing. In recent years, advancements in deep learning models have provided an opportunity to deploy vision-based sensors in buildings toward occupant-centric controls (OCC). Vision-based systems are popular devices used to monitor individual thermal sensation and satisfaction due to their capacity to non-intrusively measure skin temperature, a physiological variable that is related to thermal comfort prediction. However, this advantage of remote sensing also leads to reduced accuracy compared to conventional temperature sensors. One of the critical variables responsible for the reduced accuracy is the camera's distance from the subject, also known as 'the working distance'. As the requirement of thermal cameras in front of the targets within a fixed distance is not applicable to real operational conditions, this study proposes an experimental framework to perform real-time correction of the thermal camera's temperature for targets at the distance longer than the thermal camera's calibration distance. The prediction framework uses a low-cost thermal camera and an RGB-D module to extract the target's surface temperature and their distance to the camera, and its output can be used to assess an individual's thermal comfort based on skin temperature variation. This approach can be combined with computer vision approaches to allow the continuous detection of the occupants' faces or motion patterns, providing a holistic, multi-modal sensing solution towards occupant-centric controls.

1. INTRODUCTION

A thermal camera is a non-intrusive tool used to measure surface temperatures quantitatively and/or qualitatively by displaying warm objects against a cooler background. In thermography, thermal cameras detect infrared radiation and produce images that show temperature variations across an object. In order to measure the temperature of any target, radiometric thermal cameras measure the radiant energy and create a thermal image, in which the temperature of each pixel is determined based on the radiant energy. Microbolometers are commonly used as detectors in thermal cameras due to their lower cost. They measure radiation in the long-wavelength infrared band. The use of Non-Contact Infrared Thermometers (NCIT) and IR thermal cameras has been extended for detecting higher body temperatures in public settings during infectious disease pandemics including the recent COVID-19 pandemic. After the SARS pandemic in 2003, International Organization for Standardization (ISO), The International Electrotechnical Commission (IEC), and other governing agencies like U.S. Food and Drug Administration (FDA) developed standards to ensure the success of relevant screening programs (IEC, 2017; FDA, 2019). Medical purposes require high-accuracy thermal cameras, however, there have been attempts to use low-cost thermal cameras to capture the variation of skin temperature parameters to address occupants' comfort status, paving the way to extend the use of such technologies for human comfort studies (Li *et al*., 2018). However, the use of thermal cameras also includes uncertainties, such as the emissivity of the target, intrinsic errors, and systematic errors in the measurement procedure. To obtain the actual temperature from the apparent temperature measured by thermal

cameras, it is required to compensate for the emissivity of the measured object, while there has been research proving that changing the working distance and angle of view of a thermal camera compared to the factory-calibrated values has a negative impact on accuracy. More specifically, (Cheung et al., 2012) experimental results showed that increasing the working distance between the target and the camera decreases the reading temperature by 0.26∘ C per meter, while (Litwa, 2010) showed that, as long as the angle of view remains lower than 50 degrees, the temperature measurement results can be reliable. In that direction, correction models were proposed to compensate for the effect of distance and angle of view. Zhang et al. (2016) proposed a theoretical formula to investigate the effect of the angle of view and working distance on the accuracy of thermal cameras. The proposed theory was validated by fitting experimental data to blackbody temperature. The proposed distance correction theory applied two working distance ranges. For the working distance of less than 7 meters, a linear relation was considered for the distance correction factor, however, a quadratic relation was proposed for the correction factor for distances larger than 7 meters. Gutierrez (2020) study was the first attempt to use low-cost handheld thermal cameras for distance correction experiments. Although the low-cost thermal cameras included higher noise and less accuracy, their compensation formula based on working distance and angle of view was able to improve thermal camera accuracy from a range of (-2.56°C to +2.31°C) at the baseline to a range of (-1.44°C to +1.6°C) for the narrow working distances considered in the study (10-50 cm). Also, Li et al. (2019) proposed a linear model for distance compensation of low-cost thermal cameras within 0.8 and 2 meters working distance while using humans as the target.

As demonstrated in a previous study, high-cost instruments such as an expensive thermal camera and/or a black body target were used for distance calibration. Human targets are also used for camera calibration purposes when using a low-cost thermal camera that cannot provide a uniform and constant temperature target.

This proven dependency of accuracy on working distance pointed out the fact that automatic distance detection is the next milestone required for the integration of thermal cameras as automated smart sensing systems. RGB-depth sensors are primarily used for distance detection, but they are also useful in human-centered applications, aiding in human detection and tracking. To be utilized in a system with a thermal camera, a registration process is required to locate the corresponding points for the two sensors that have different optical characteristics and are not in the exact same position. The computation time, complexity, and required robustness of the registration method used can all differ. The research on multi-modal registration approaches has advanced rapidly, with studies on the fusion of thermal and RGB cameras ranging from medical applications (Gonzalez-prez et al.,2021; Muller et al., 2018; Ma e al.,2019) to low-cost 3D thermal model reconstruction for monitoring and inspection purposes (Yang et al.,2018; Aryal et al., 2019). A comparison of four different feature and intensity-based image registration algorithms for diabetic foot monitoring (González-Pérez et al., 2021) found that using feature-based algorithms that rely on feature point detection can lead to higher errors, especially for low-cost thermal cameras. In contrast, intensity-based registration performed better than feature-based however they add the requirement of image segmentation.

Multi-modal stereo cameras have also been utilized in the field of occupant-centric building control applications (Li et al., 2019; Aryal et al., 2019) to measure human face skin temperature and comfort or towards glare assessment and controls (Kim et al., 2019). Off-the-shelf low-cost thermal and RGB cameras with calibration-based registration were used to extract temperature information from an object detected in an RGB image (Li et al.,2019), while the 2D transformation matrix was obtained by selecting control points for thermal and RGB cameras registration (Aryal et al.,2019).

Despite the previous research on multi-modal camera integration and correction methods for low-cost thermal cameras, the validity and applicability of the experimental methods should be investigated further. In this paper, a dual-camera registration and distance correction experiment for low-cost off-the-shelf thermal cameras is designed for various measuring distances. The stereo-calibration process for image registration and the influence of the working distance on thermal camera measurement accuracy is obtained and analyzed using the experimental results. For thermal camera calibration, we proposed a low-cost framework that did not require the use of a black-body or a human target. Based on our results, the proposed distance correction formula helps in reducing the thermal camera's temperature measurement error, while the fusion of the depth sensor allows for this correction to be seamless and automatic in real-world implementations. The distance correction model and image registration of thermal and RGB cameras will be valuable for vision-based human thermal comfort assessment, while the accuracy of low-cost thermal cameras remains low.

2. METHODOLOGY

This study employs two techniques to establish a framework that will allow assessing comfort using a low-cost-thermal camera and a depth sensor: (i) Computer vision to register two cameras so that the corresponding pixels

from two different cameras can be found; and (ii) Distance Calibration of a thermal camera to compensate for the effect of distance on thermal camera accuracy through a correction function. Below, the main components are summarized:

a. Low-cost thermal camera: A low-cost off-the-shelf thermal camera with an uncooled Vox microbolometer detector was chosen for this study. This long-wave infrared camera (LWIR) can detect electromagnetic wavelengths in the range of 8 to 14 μm and produces images with a resolution of 160 by 120 pixels, the thermal camera's radiometric feature can measure the temperature of each pixel based on the intensity of the infrared signal received by the camera (Table 1).

Table 1: Thermal camera specifications

Features	Descriptions
Dimensions	11.8x12.7x7.2mm
Array Format	160x120 pixels
FOV Horizontal	56
FOV Diagonal	71
Radiometric accuracy	±5∘C or ± 5% of reading in the working distance

The camera (Figure 1 left) was hosted in a custom 3D-printed case and connected to a chipset-on-board computer through a breakout board providing 3.3 input voltage for the camera, and the camera's output displays each pixel's temperature in Kelvin.

Figure 1: Thermal capture prototype (left) – Dual camera setup (right)

b. RGB-D Sensor: To extract depth and RGB images, a stereo-vision depth camera was utilized (Table 2). After capturing images from the left and right IR sensors, the sensor undergoes disparity and triangulation to calculate depth data.

Table 2: RGB-D sensor specifications

Features	Descriptions
Operating Range	0.3-3m
Depth FOV	87x58
RGB FOV	69x42
Depth resolution	Up to 1280x720
RGB frame resolution	Up to 1920x1080
Depth accuracy	<2% at 2m

The proposed dual-camera system consists of a thermal camera and RGB-D sensor rigidly placed on a mounting plate (Figure 1 right). As the resolution and Field of View (FOV) for these two image sensors differ, image registration was a necessary step to identify the corresponding pixels in their resulting images, as described below.

2.1 Sensor Fusion

For a multi-modal system, two different image registration approaches were used: feature-based and calibration-based. Key points were detected in feature-based, and then feature mapping and image transformation were discovered. The information from the two cameras, including their intrinsic and extrinsic matrices, is required for calibration-based image registrations. The Zhang (2000) method was used to map 3D coordinates into 2D image planes, with the camera modeled as a pinhole camera, in order to determine the intrinsic and extrinsic matrices.

The intrinsic matrix expresses the relation between 3D camera coordinates and the 2D image coordinates, while the extrinsic matrix shows the relation between the 3D world coordinates and the 3D coordinates of the camera. The extrinsic matrix includes rotation and translation matrices.

Figure 2 shows a schematic diagram for a stereo camera, where P is a part of a scene in 3D world coordinates and captured with a thermal camera on an image plane IR at point P_{IR} and a RGB-D camera on an image plane RGB at point P_{RGB}.
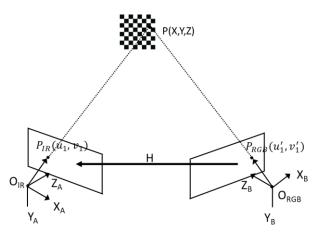

Figure 2: Stereo multi modal camera geometry

The coordinates of the corresponding point in image plane of IR as P_{IR} (u_1, v_1) and RGB as P_{RGB} (u'_1, v'_1) are obtained from the pinhole camera model (Zhang, 2000) in a stereo calibration process, Z_1 is the scaling factor. The Homography matrix shown in Equation (1), describes the transformation of points from one image to another image when the points lie in a plane. To find the Homography matrix, at least four pairs of corresponding points from thermal and RGB cameras are required (Swamidoss et al.,2021):

$$Z_1 \begin{bmatrix} u_1 \\ v_1 \\ 1 \end{bmatrix} = \begin{bmatrix} H_{11} & H_{12} & H_{13} \\ H_{21} & H_{22} & H_{23} \\ H_{31} & H_{32} & H_{33} \end{bmatrix} \begin{bmatrix} u'_1 \\ v'_1 \\ 1 \end{bmatrix}, H_{33} = 1 \tag{1}$$

$$u_1 = \frac{H_{11}u'_1 + H_{12}v'_1 + H_{13}}{H_{31}u'_1 + H_{32}v'_1 + 1} \tag{2}$$

$$v_1 = \frac{H_{21}u'_1 + H_{22}v'_1 + H_{23}}{H_{31}u'_1 + H_{32}v'_1 + 1} \tag{3}$$

If we have "i" corresponding points from stereo-calibration, we can change the form of Equations (2) and (3) to Equation (4), which incorporates all corresponding points:

$$
\begin{bmatrix} u_i^{'} & v_i^{'} & 1 & 0 & 0 & 0 & -u_i u_i^{'} & -u_i v_i^{'} \\ 0 & 0 & 0 & u_i^{'} & v_i^{'} & 1 & -v_i u_i^{'} & -v_i v_i^{'} \end{bmatrix}_{2iX8} \begin{bmatrix} H_{11} \\ H_{12} \\ H_{13} \\ H_{21} \\ H_{22} \\ H_{23} \\ H_{31} \\ H_{32} \end{bmatrix}_{8x1} = \begin{bmatrix} u_i \\ v_i \end{bmatrix}_{2iX1} \tag{4}
$$

In order to find the Homography matrix, the Least Square method is used to solve Equation (4).
For the stereo calibration experiment, an aluminum plate with 50cm x 40cm dimension with a chessboard pattern (8x7) on it was used. The square pattern on the chessboard had a 5cm dimension. Ten image pairs were taken from an aluminum chessboard plate by RGB-D and thermal camera in different orientations and distances from the camera. The results of the calibration are presented in Section 3.

2.2 Distance Calibration

To perform calibration for different working distances, the first step required setting up an experiment where temperature can be measured and controlled. To that end, a reptile pad was utilized, enabling to maintain the temperature at the desired temperature for an hour. As our end objective for this framework is the use for human skin temperature screening, this reptile pad was considered to be a good fit able to provide a temperature of 30-40 °C. The reptile pad was attached to an aluminum sheet painted with a flat black color spray to avoid reflection. The process started once the aluminum temperature reached 36°C, with the plate temperature being monitored through T-type thermocouples. The aluminum plate maintained its temperature within a margin of approximately 36°C, with the minor fluctuations being a result of the fluctuations of the reptile pad. The camera was fixed in place and the working distance with the target was varied from 50 cm to 2 meters in 10 cm increments. As a result, 160 thermal images were captured and processed to obtain a correction function as presented in Section3.

3. RESULTS AND DISCUSSION

Figure 3 shows the detected points of the reference chessboard by the thermal camera (camera 1) and RGB camera (camera 2) that were used for the calibration process. Despite the low resolution of the low-cost thermal camera, the mean re-projection error was kept within 0.1 pixels (Figure 4). This shows the calibration was able to detect the corners of the chessboard for both the thermal and RGB images with high accuracy.
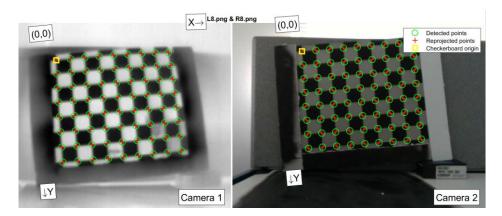

Figure 3: Detected and re-projected points after stereo calibration
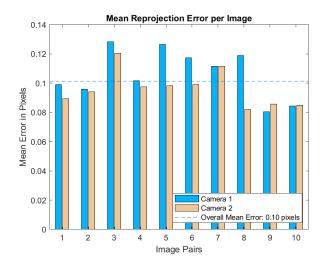
Figure 4: Mean re-projected error in pixels

The relative position and rotation of these two cameras with respect to the target orientation are shown in Figure 5, while Figure 6 reflects through rectified images how the corresponding points of thermal and RGB images are in the same row coordinates.
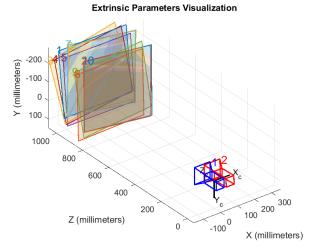

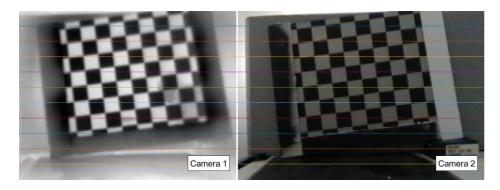**Figure 5:** Extrinsic parameter visualization

Figure 6: Epipolar geometry of rectified images

The Homography matrix is calculated using the corresponding points, so by having Homography matrix, the associate points in RGB image in thermal image will be found.
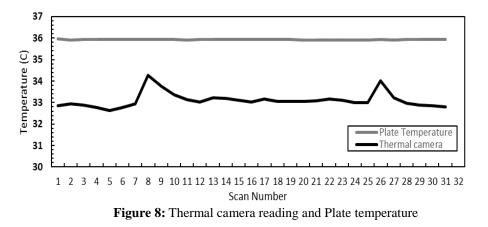
$$H = \begin{pmatrix} 1.0407 & 0.0252 & 6.42 \\ -0.0016 & 1.0460 & 8.8858 \\ 0 & 0 & 1 \end{pmatrix}$$

After the successful fusion, the distance information obtained from the RGB-D sensor will be utilized to correct the resulting temperature of the thermal imaging base on the measured distance from the camera. To that end, Figure 7 illustrates an example of the image shooting process for distance correction.

Figure 7: Experiment measurement

A noteworthy issue with low-cost thermal cameras is the occurrence of temperature peaks in standard frequencies. Figure 8 illustrates the issue, with the experience of peaks for the plate temperature reading from the thermal camera at 1m. These peaks are an inherent characteristic resulting from the Flat Filed Correction of low-cost thermal cameras and are necessary for temperature readings to cancel the impact of increasing temperature of the internal camera. After coordination with the manufacturers, these standard peaks were filtered out of the data, as they were out of the scope of our study.

Figure 8: Thermal camera reading and Plate temperature

The plate temperature was measured by calculating the average value of the region of interest (ROI) of 10x10 pixels (T_{cam}), as shown in Figure 9. The temperature reading by the thermocouples is referred to as reference temperature (T_{REF}), while the relative error is defined as the difference between the reference temperature (T_{REF}) and thermal camera reading (T_{cam}) divided by T_{REF}.
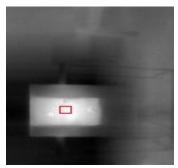
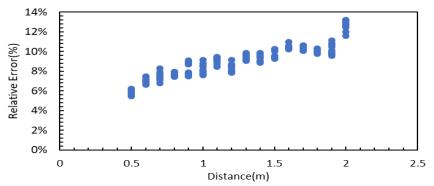**Figure 9:** ROI of 10x10 pixels in the thermal image

Figure 10: Thermal camera relative error in different working distances

As it can be observed in Figure 10, there is an increasing trend in the impact of working distance on the relative temperature error for the thermal camera. The behavior of this trend can be approximated through a linear relationship, which in turn advocates towards a correction function for the measured temperature by the thermal camera.

For our study, a regression model was used to correct the estimated temperature using thermal camera readings. The model used T_{REF} as one of the inputs (predictor variables) as well as working distance. The camera measurement was used as the response variable. After inferring the model, the inverse methodology can be used to obtain a corrected temperature based on the thermal camera reading and the working distance measurement. The result was assessed through 10-fold cross-validation that showed a RMSE of 0.28 with a standard deviation of 0.039.

The 80% of the collected data was chosen as the training dataset for linear regression model, and 20% of the data was used to validate the developed model. The structure of the developed model is shown in Equation (6), where D is the working distance and T_{REF} is the temperature measured by the thermocouple. The model results are shown in Table 3.

$$T_{cam} = Const + (\alpha_1)*(D) + (\alpha_2)*(T_{REF}) \tag{6}$$

Table 3: Model Parameters

Predictors	Values	P-Value
Const	12.083	0.002
Distance Coefficient (α_1)	-1.168	0.000
Reference Coefficient (α_2)	0.616	0.000
R2	0.776	
Adjusted R2	0.772	

T_{Corrected} (or T_{REF} in Equation (6)) is the thermal camera's distance-corrected temperature derived from Equation (6). As a result, the corrected camera reading is estimated using Equation (7), which includes the distance and thermal camera reading.

$$T_{corrected} = \frac{1}{(\alpha_2)} \left[-Const + T_{cam} - (\alpha_1)*(D) \right] \tag{7}$$

Figure 11 shows that using the distance corrected formula on the validation dataset can reduce relative error from 9% to 0.9%.
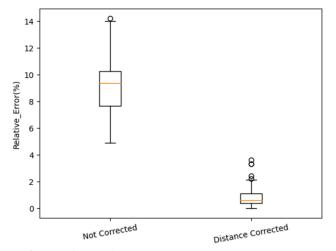

Figure 11: Relative error of thermal camera reading

4. CONCLUSION

This paper presented the formulation of a thermal imaging system consisting of a thermal camera and a depth sensor, aiming to address the deficiencies of thermal imaging with respect to errors due to varying target working distances. The system, aided by a newly developed distance correction formula, was proven to reduce the thermal camera's measurement error from 9% to 0.9%. The overarching goal and the future work of the authors is for this vision-based system to be able to provide non-intrusive information about occupant thermal comfort. Flexible temperature sensors of adequate accuracy as the proposed one can be used in that context to capture temperatures of the occupants' skin or even surrounding surfaces, which can serve as feedback in future occupant-centric building controls. Currently, the authors are also working on adding face or video patterns detection features to this framework, further expanding its usability as an integrated human comfort feedback device.

ACKNOWLEDGEMENT

REFERENCES

Aryal, A., & Becerik-Gerber, B. (2019, November). Skin temperature extraction using facial landmark detection and thermal imaging for comfort assessment. In Proceedings of the 6th ACM International Conference on Systems for Energy-Efficient Buildings, Cities, and Transportation (pp. 71-80).
Cheung, B. M. Y., Chan, L. S., Lauder, I. J., & Kumana, C. R. (2012). Detection of body temperature with infrared thermography. Hong Kong Medical Journal, 18(4 Suppl 3), 31-34.

Enforcement policy for telethermographic systems ... - FDA. (n.d.). Retrieved April 15, 2022, from https://www.fda.gov/media/137079/download.

González-Pérez, S., Perea Ström, D., Arteaga-Marrero, N., Luque, C., Sidrach-Cardona, I., Villa, E., & Ruiz-Alzola, J. (2021). Assessment of registration methods for thermal infrared and visible images for diabetic foot monitoring. Sensors, 21(7), 2264.

Gutierrez, E., Castañeda, B., & Treuillet, S. (2020, February). Correction of temperature estimated from a low-cost handheld infrared camera for clinical monitoring. In International Conference on Advanced Concepts for Intelligent Vision Systems (pp. 108-116). Springer, Cham.

IEC80601-2-59:2017.ISO.(2022,March14).Retrieved April 15, 2022, from https://www.iso.org/standard/69346.html

Kim, M., Konstantzos, I., & Tzempelikos, A. (2019). A low-cost stereo-fisheye camera sensor for daylighting and glare control. Journal of Physics: Conference Series. Vol. 1343, No. 1, p. 012157). IOP Publishing.

Li, D., Menassa, C. C., & Kamat, V. R. (2018). Non-intrusive interpretation of human thermal comfort through analysis of facial infrared thermography. Energy and Buildings, 176, 246-261.

Li, D., Menassa, C. C., & Kamat, V. R. (2019). Robust non-intrusive interpretation of occupant thermal comfort in built environments with low-cost networked thermal cameras. Applied energy, 251, 113336.

Litwa, M. (2010). Influence of angle of view on temperature measurements using thermovision camera. IEEE Sensors Journal, 10(10), 1552-1554.

Ma, J., Ma, Y., & Li, C. (2019). Infrared and visible image fusion methods and applications: A survey. Information Fusion, 45, 153-178.

Müller, J., Müller, J., Chen, F., Tetzlaff, R., Müller, J., Böhl, E., ... & Schnabel, C. (2018). Registration and fusion of thermographic and visual-light images in neurosurgery. IEEE Transactions on Biomedical Circuits and Systems, 12(6), 1313-1321.

Nakagawa, W., Matsumoto, K., Sorbier, F. D., Sugimoto, M., Saito, H., Senda, S., ... & Iketani, A. (2014, September). Visualization of temperature change using RGB-D camera and thermal camera. In European Conference on Computer Vision (pp. 386-400). Springer, Cham.

Swamidoss, I. N., Amro, A. B., & Sayadi, S. (2021). Systematic approach for thermal imaging camera calibration for machine vision applications. Optik, 247, 168039.

Yang, M. D., Su, T. C., & Lin, H. Y. (2018). Fusion of infrared thermal image and visible image for 3D thermal model reconstruction using smartphone sensors. Sensors, 18(7), 2003.

Zhang, Y. C., Chen, Y. M., Fu, X. B., & Luo, C. (2016). A method for reducing the influence of measuring distance on infrared thermal imager temperature measurement accuracy. Applied Thermal Engineering, 100, 1095-1101.

Zhang, Z. (2000). A flexible new technique for camera calibration. IEEE Transactions on pattern analysis and machine intelligence, 22(11), 1330-1334.